



Through the Eye of the Mirror,

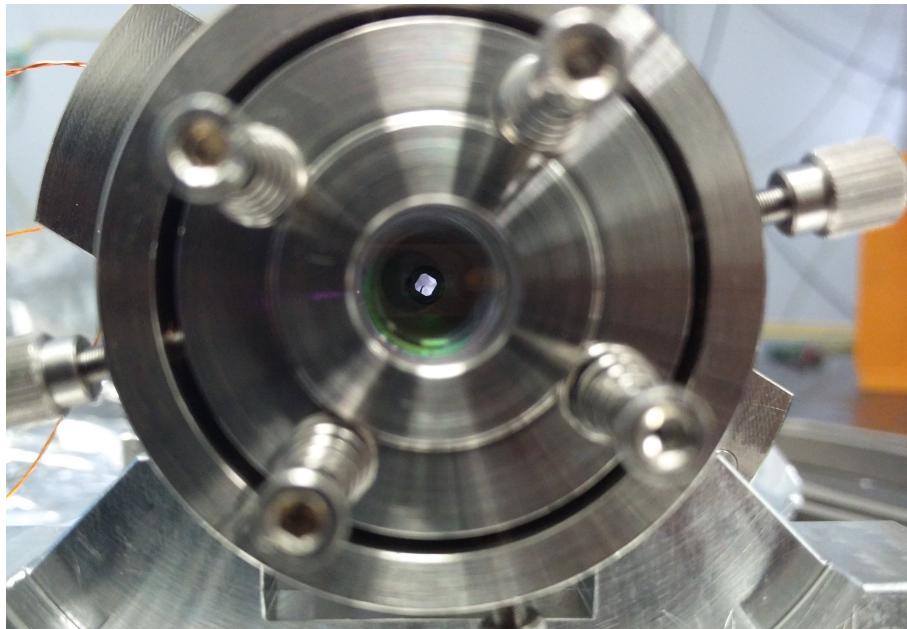
Characterizing and Testing

A New Membrane in the Middle Cavity

and

In-Situ Absorbance and Thermal Gradient
Measurements

Within Phononic Crystal Optomechanical Membranes



THESIS
submitted in partial fulfillment of the
requirements for the degree of
MASTER OF SCIENCE
in
PHYSICS

Author : T.M. Fuchs
Student ID : S1408852
Supervisor : Prof.dr. D. Bouwmeester
Dr. W. Löffler
V. Fedoseev MSc.
2nd corrector : Prof.dr.ir. T. Oosterkamp

Cover picture: Front view photograph of the new optical cavity tested in this thesis. The membrane can be seen through the front mirror, in the middle of the cavity. The needle used to excite and drive the membrane is visible over the center of the membrane as well. Finally, one can see the screws used to position the end mirror on the x axis, with the end plate held onto the cavity through the four screws and springs on the front of the end plate.

Leiden, The Netherlands, August 30, 2019

Through the Eye of the Mirror,

Characterizing and Testing

A New Membrane in the Middle Cavity

and

In-Situ Absorbance and Thermal Gradient Measurements

Within Phononic Crystal Optomechanical Membranes

T.M. Fuchs

Huygens-Kamerlingh Onnes Laboratory, Leiden University
P.O. Box 9500, 2300 RA Leiden, The Netherlands

August 30, 2019

Abstract

In this thesis, we characterize and test a new MiM cavity for use in the Bouwmeester Optomechanics group. The cavity seems stable over time, though alignment offers some issues. The tip/tilt alignment of the membrane was achieved to within 700 arcs eventually however. We also explore the use of finesse measurements to determine the absorbance of our membranes. We conclude that optical ring down measurements are preferable in our system and suspect that the PSG4 membranes have higher absorbance as compared to later generations. We present a scheme to determine the thermal gradient of our membrane in-situ, without any modifications required to the principle of the system. We do find, however, that the measurement is very sensitive to drift of the laser detuning. Finally, we explore the observed short term drift in our mechanical mode frequencies. We suspect the thermal expansion of some part of the system of adding additional strain to the membranes, and in doing so raising their mode frequencies, though the exact pathway remains unclear.

Keywords: MiM, Optomechanics, Quantum Optomechanics, Optical Cavity, Mechanical Resonator, Membrane, Phononic Crystal, Thermal Gradient, Quantum Superpositions, Quantum Mechanics, Classical Mechanics, Thermal, Decoherence, Absorbance

Contents

1	Introduction	1
1.1	Quantum Superpositions and the Cat	1
1.2	The Transition: a Quantum and a Classical Regime	2
1.3	Exploring the Transition: Bounds and Control	4
1.4	The Membrane in the Middle System	5
1.5	In This Thesis	6
2	Theory	7
2.1	Optomechanics and the Membrane in the Middle System	7
2.1.1	Optical Cavities	7
2.1.2	Mechanical Resonator	9
2.1.3	Optomechanical Coupling Between a Cavity and a Membrane	12
2.2	Additional Mechanics of Interest to Membrane Optomechanics	13
2.2.1	Thermal Expansion	13
2.2.2	Absorption	14
3	Methods	16
3.1	The Current Set-Up	16
3.1.1	Optical Cavity	16
3.1.2	Kinematic Plate and Membrane Holder	17
3.1.3	The Membrane	18
3.1.4	The Laser Lab	20
3.2	The New Set-Up	22
3.3	Absorbance Measurement	24
3.4	Thermal Gradient Measurement	25
4	Results and Discussion	27
4.1	The New Set-Up	27
4.1.1	First Alignment	27
4.1.2	Final Alignment	27
4.1.3	Empty Cavity Finesse	29
4.1.4	MiM	29
4.1.5	MiM Finesse	30
4.1.6	Tip/Tilt Alignment	30
4.1.7	Vacuum	31
4.1.8	Membrane Modes PSG5.1.1,3 and PSG5.2.1	31
4.1.9	Bandgap	32
4.1.10	Quality Factor	32

CONTENTS

4.1.11	Frequency Dragging and Optical Driving	33
4.2	Membrane Absorbance Measurements	34
4.3	Thermal Gradient Measurements	36
4.4	Mode Frequency Drift	37
5	Conclusions	41
5.1	The New Set-Up	41
5.2	Membrane Absorption	41
5.3	Thermal Gradients	42
5.4	Mode Frequency Drift	42
6	Acknowledgements	43

CHAPTER 1

Introduction

Since its first formulation, quantum mechanics has moved from an oddity required to explain away the UV catastrophe and understand the photoelectric effect, to the most active area in physics, being studied by most physicists in one shape or another.

This interest and push into quantum mechanics has also led to an increased interest on the application side and from industry. Think of, for example, applications such as chip design and quantum computing. This in turn creates more demand for research into the field, as to keep up with the request for knowledge from industry.

That is not to say that interest is purely application driven. Being the foundation of our current physical understanding, quantum research is very interesting from a fundamental research standpoint as well.

Fact of the matter is that quantum mechanics has become a very important part of modern technology and research, and will continue to become even more so with increasing progress.

1.1 Quantum Superpositions and the Cat

A central aspect of quantum mechanics is the concept of “quantum superpositions”, being one of the main distinguishing factors between classical and quantum mechanics. These “superpositions” are also one of the central parts of so called quantum speed ups in quantum computing, wherein the supposed performance gain lies between quantum and classical systems [1].

What is meant with a “quantum superposition” is a system (a particle or set of particles) being in a state (configuration of parameters such as momentum, position, energy, etc.) that is the sum of multiple other states. The famous example being Schrödinger’s cat, a thought experiment of Erwin Schrödinger [2]: suppose we were to put a cat in a closed box. Within this box, we also placed a Geiger counter, a hammer, a vial of cyanide, and a trace amount of radioactive material. The hammer is attached to the Geiger counter in such a way that, when the counter detects the decay of our radioactive material, it will release, and smash the cyanide vial, see figure 1.1.

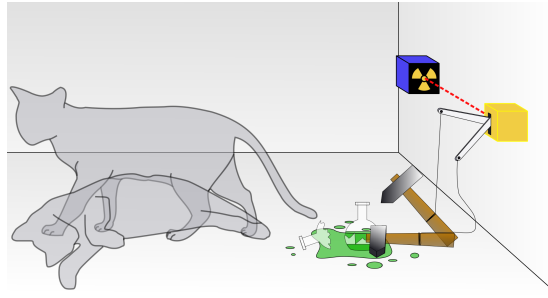


Figure 1.1: Schematic representation of Schrödinger's cat thought experiment as described in the text.

Now, clearly, the cyanide releasing will kill the cat *. However, radioactive decay is a stochastic (random) process, meaning that, given the small amount of material we have, it is not at all guaranteed that the Geiger counter will register an event in a certain time period. Without observing what happened inside the box, there would be no way for us to know whether the cat has died. Classically, this just means we don't know whether the cat is dead (system in state 2) or still alive (system in state 1). The system is in either one of those states, we just don't know which. In quantum mechanics, however, the sum of these states (dead+alive), is again a valid state, being a superposition state of state 1 and state 2, artistically represented in a way similar to how it would be done in the field in figure 1.2.

$$\frac{1}{\sqrt{2}}|\text{alive}\rangle + \frac{1}{\sqrt{2}}|\text{dead}\rangle$$

Figure 1.2: Artistic representation of the super position state known as a "cat state", after the Schrödinger's cat thought experiment as described in the text. It represents the (normalised) state vector, denoted in (bra-)ket notation of the cat state, being a super position of the "alive" state and the "dead" state.

Figure taken from D. Ellerman (2017) "From Abstract Entities in Mathematics to Superposition States in Quantum Mechanics", accessible online at [arXiv:1701.07936](https://arxiv.org/abs/1701.07936) [quant-ph][4]

1.2 The Transition: a Quantum and a Classical Regime

This idea of cats being both dead and alive at the same time might sound weird, since this is not what we observe in everyday life. Everything around us seems firmly in one state at a time, without real ambiguity given proper observation: trees sway in the wind in one way at a time, rather than swaying left first then

*It is, after all, quite deadly, [3]

right, and right first, then left, simultaneously. The world at our scale, seems firmly classical.

From experimental tests, however, this seems to not be the case at the smaller scales in controlled experiments: quantum superpositions are real [5]. If we launch consecutive electrons, one at a time, through a barrier with two slit, at a phosphorous screen placed some ways behind the barrier, and we only observed the screen, we observed something remarkable: rather than showing two lines, representing a path through either of the two slits towards the screen, we observe an interference pattern on the screen [6], as depicted in figure 1.3.

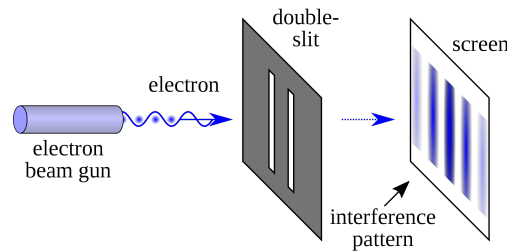


Figure 1.3: Schematic representation of the double slit experiment as described in the text.

This represents the electron effectively going through both slits, and then interfering with itself in a wavelike fashion. That is to say: the electrons are in a superposition of going through slit 1, and going through slit 2, on their way to the screen.

Now if we observe the barrier as well (so that we would know which slit the electron went through), this pattern disappears: we are left with two single slit patterns. Somehow, the observations forced our system out of it's quantum superposition state, into a classical state.

It remains unclear, however, what exactly causes this divide between quantum and classical systems. In observing our electron going through the slits, we coupled a very large system into our small electron system: we went from a system effectively made up of a single electron, to a system in which we could display which slit that electron went through on a computer screen, consisting of millions upon millions of electrons. It seems that our system lost it's "quantumness" through coupling to the environment.

In a slightly less vague way of putting it: quantum systems form and evolve in time as wave functions. These waves have a phase, among other properties. Through interactions with the environment, this information on the phase of our system becomes linked and distributed into other systems. Some process causes a loss of this information in each system, leading to the eventual decay of the wave, causing our system to decohere into a classical state.

Given the importance of information on this process (which causes a loss of quantum coherence) for our fundamental understanding of the world we live in, and the possible importance of quantum super positions (which can only exist in systems that are quantum mechanically coherent) in modern technology, it is clear that it is of utmost importance to carefully explore this transition from the quantum mechanical regime, to the classical regime.

1.3 Exploring the Transition: Bounds and Control

There have been many proposed mechanisms for this loss of quantum coherence. An important suspect for this mechanism is gravitationally induced wave function collapse, in which significantly large disturbances of space-time lead to the collapse of the super position causing said disturbances [7]. To study this type of mechanism and any other type of mechanism, it is important to very carefully control what constitutes as our system. For mechanisms involving gravity, the size, and therewith associated mass, of the system is of utmost importance as well. The challenge at hand then becomes to have systems that can be very carefully controlled, but whose states can be maximally isolated from the environment, and steadily increasing the size of said systems. By doing this, upper bounds can be established on super position states, and simple, large systems would aid in more easily exploring and understanding what is happening at the cusp of any transition that is discovered.

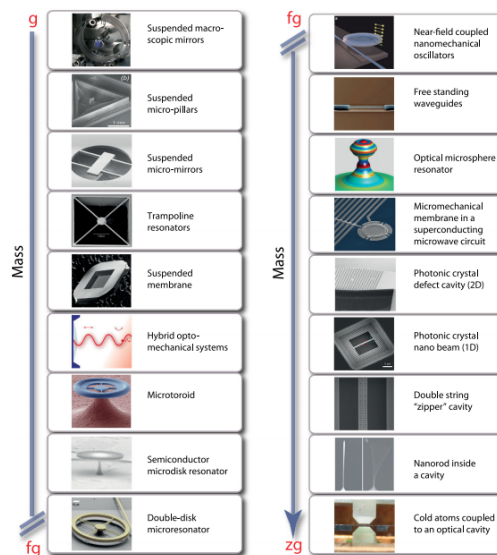


Figure 1.4: Photographic representation of different optomechanical resonator systems, taken from M. Aspelmeyer, T.J. Kippenberg and F. Marquardt, "Cavity optomechanics", *REVIEWS OF MODERN PHYSICS*, VOLUME 86, OCTOBER-DECEMBER 2014. [8]

Achieving large levels of control whilst simultaneously isolating the system from the environment is in itself a large challenge, since control can only be accomplished through coupling through some other system. The remainder of the challenge then lies in having a system whose mass can be made sufficiently large whilst still being easy to isolate from the environment. An ideal candidate for such a system is found in optomechanics. In such systems, the control can be readily done using optical means such as laser pulses, which, after the state control, can be rapidly turned off/reduced in power, to effectively reduce/switch off the coupling with the environment through that pathway at

least. Furthermore, the mass of the mechanical part of the system can be easily increased and controlled. What remains is the isolation of the mechanical system from the environment, and the development of optical techniques to address the system. These optomechanical resonator systems are currently being developed in many shapes and most importantly, mass ranges, as depicted in figure 1.4

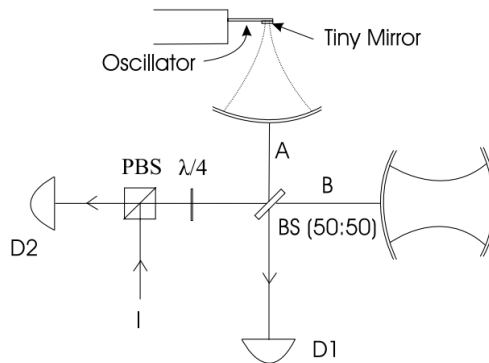


Figure 1.5: Schematic representation of the in 2003 proposed experiment, taken from the paper [9]. In the experiment, a single photon is brought in a superposition of being in arm A and arm B through a 50:50 beamsplitter. In arm A, it is coupled to a mirror mounted on a mechanical oscillator through the radiation pressure exerted on said mirror by the photon. This causes the system to evolve into a superposition state of two different equilibrium points for the end mirror (driven by radiation pressure, or not driven). The time evolution of this superposition and thus the decoherence of this massive state, is then inferred from the interference of the photon leaving the system again. The cavity in arm A is solely there to enhance the radiation pressure of the single photon.

1.4 The Membrane in the Middle System

Following an experiment proposed in 2003 [9] involving a Michelson interferometer with one of the end mirrors mounted on a mechanical oscillator and further developments to the idea, the Bouwmeester group now works on Membrane in the Middle (MiM for short) systems, first studied by Thompson et al [10]. These systems consist of a (translucent) membrane placed between two high quality mirrors, forming an optical cavity, with a membrane in the middle (hence the name). The coupling between the optical system (cavity with photons) and the mechanical system (membrane with phonons) arises from a frequency shift of the optical cavity mode caused by a change in the effective pathlength of the cavity as a function of the membrane displacement. This will be further explained in the *Theory* section of this thesis.

Since we want to study the quantum mechanics of the system, we will need to bring the system into a quantum mechanical state. To do so, the system must be cooled down, to reduce the thermal decoherence rate of the system (the

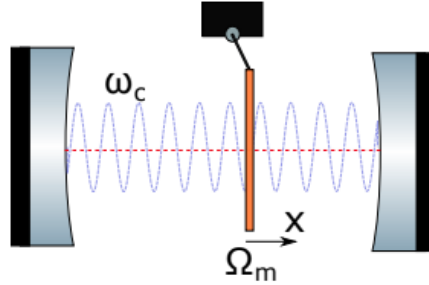


Figure 1.6: Diagram for a generic Membrane in the Middle system, taken from the thesis of S. Sonar [11]

rate at which thermal motion/phonons causes the system to decohere through damping of the mechanical mode) and isolate it from outside vibrations. This thesis will not focus on this cooling and isolation, though the current implementation of both will be discussed in the *Methods* section. Rather, it focuses on validating the effectiveness of said cooling, so as to establish whether the cooling is sufficient, and if it is not, where the issues lie.

1.5 In This Thesis

In the next section, *Theory*, we will briefly explain the theory underlying the optomechanical system and go over the thermodynamics and mechanics that is of interest to this thesis. Meanwhile, we will discuss the cooling schemes and the thermal properties of the system and their importance.

In the following section, *Methods*, we will introduce the methods developed to probe some of these thermal properties, namely the determination of the membranes optical absorbance and a method of probing the existence of a possible temperature gradient in the membrane using no additional means other than the current probing used to read out the system. Before doing so, we will start the section off by introducing the set-up currently in use.

Afterwards, in the section *Results and Discussion*, we will discuss a new set-up, designed to reduce positional drift of the membrane, observed in the previous set up. This drift could cause a drift in cavity finesse and detuning, in turn possibly leading to changes in optomechanical cooling and heating effects on the membrane. We will then continue to the first tests of the methods developed and discuss these results. In this section, we will also discuss the observed drift in the mechanical mode frequency of the membrane over relatively short timescales.

After this, a brief conclusion will follow in the *Conclusion* section.

CHAPTER 2

Theory

In this section, we will go over the theory underlying this thesis. We will start with a brief introduction to Membrane in the Middle systems. This discussion will be kept brief, merely introducing and describing the effects in use, referring the reader to other works written both by the Bouwmeester group and reviews of Optomechanics not written by the group for a more complete and mathematically rigorous derivations and explanations [8, 10–12].

2.1 Optomechanics and the Membrane in the Middle System

As noted before, optomechanics entails the coupling of mechanical and optical systems. This coupling is enacted through the radiation pressure exerted on mechanical systems by light: although light has no mass, it does carry momentum, and thus exerts a force on a surface it is either absorbed, reflected, or emitted by/from.

Nominally, this force is marginal for any mechanical system of appreciable scale. Therefor, it is usually enhanced. This is done through the use of optical resonators, or more commonly, optical cavities. This is referred to as cavity optomechanics.

2.1.1 Optical Cavities

The basic idea of an optical cavity is to make light bounce between two surfaces as often as possible, thus enhancing the amount of light that is present within the cavity at a set time. Of course, the truth of the matter is slightly more complex, though not by much.

Light being a(n electromagnetic) wave, means that the light in the cavity will interfere with earlier and later parts of the wave if it is to be reflected between the two surfaces. It follows from the superposition* principle for linear

*Not a quantum superposition this time, though those follow from this principle. As noted in the introduction, quantum systems are described by so called wave functions, mathematically

systems that the resulting field in the cavity will be the sum of all the waves propagating both ways within the cavity.

This interference effect means that, to effectively increase the power of light within the cavity, the wavelength of the light to be amplified should be matched to the cavity: it should form a standing wave within the cavity, so as to ensure that over all the consecutive bounces, the light will still interfere constructively (all peaks matching up and thus being added up).

Mathematically, this can be summarized as

$$L = \frac{m\lambda}{2}, \quad (2.1)$$

where L is the separation between the surfaces, m denotes the integer number of bounces called the order, and λ is the wavelength of the light. Obviously, this can be solved for a set of λ and m , with constructive interference occurring at intervals of the so called Free Spectral Range (FSR for short),

$$\Delta\omega_{FSR} = \frac{c}{L}. \quad (2.2)$$

When looking at the transmission signal of a cavity when the input wavelength is scanned, this FSR shows up as the part of the spectrum where the transmission is free of much transmission: the spectrum will show peaks separated by the FSR.

As said at the start of this subsection, to enhance the light, we want to bounce the light as often as possible. An important measure for this is the finesse of the cavity. The finesse is a measure for how often the light will bounce inside the cavity before being lost due to scattering losses and leakage out of the end mirrors. It is given by the ratio of the FSR to the cavity linewidth, κ , which is in itself a measure for the loss rate of photons (being the inverse of the photon lifetime within the cavity):

$$\mathcal{F} = \frac{\Delta\omega_{FSR}}{\kappa}. \quad (2.3)$$

Having introduced these basic quantities for (classical) cavity performance, we refer the reader to other works for a more formal quantum mechanical treatment of the cavities Hamiltonian and photon occupation number, through master equations or input-output theory [8]. For this thesis, it suffices to summarize that the expectation value of the field amplitude in the cavity will be given, provided some assumptions, by

$$\langle \hat{a} \rangle = \frac{\sqrt{\kappa_{ex}} \langle \hat{a}_{in} \rangle}{\kappa/2 - i\Delta}, \quad (2.4)$$

where κ_{ex} is the loss rate due to the coupling of light into the cavity; κ is the total loss rate of the system, comprising of κ_{ex} and the rate of all other losses, κ_0 ; $\langle \hat{a}_{in} \rangle$ is the amplitude of the coherent, monochromatic driving laser incident on the cavity; and Δ is the detuning of said lasers frequency with respect to the cavity mode being driven. Taking the inner product of this expectation value with its own complex conjugate, we find the photon occupation number.

given by the Schrödinger equation. This is a linear equation, therefor meaning that the quantum states also follow the superposition principle: sums of states are again real states, leading to quantum superpositions.

$$\bar{n}_{cav} = \langle \hat{a}^\dagger \hat{a} \rangle = \frac{\kappa_{ex} |a_{in}|^2}{(\kappa/2)^2 + \Delta^2} \quad (2.5)$$

This function is shown plotted for arbitrary values in figure 2.1. It clearly depicts the lorentzian lineshape of the cavity modes, growing sharper with higher cavity finesse, or, equivalently, reduced loss rates. Quantities discussed before are annotated in the figure.

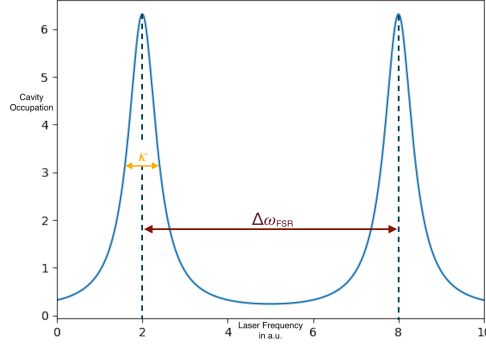


Figure 2.1: Schematic representation of cavity occupation as function of laser wavelength. The dashed lines at $x = 2$ and $x = 8$ denote the cavity modes, separated by a single FSR. The Full Width at Half Maximum (FWHM for short) corresponds to the cavity loss rate, κ .

Having thus enhanced the cavity photon occupation, consequently the resultant radiation pressure, and therefore the coupling, we will now proceed to the mechanical part of the equation.

2.1.2 Mechanical Resonator

Similar to as in the *Optical Cavities* subsection, we refer the reader to a review paper for a more rigorous mathematical derivation of the following results. In the following, we will merely provide some main equations, and discuss their physical implications. Through doing so, we will introduce some important characteristics of our system.

Given a mechanical system free to vibrate, constrained only at the edges (i.e.: a membrane, a drum, etc.), we can identify multiple ways in which the system will naturally vibrate. These different ways are referred to as the vibrational modes, and they can be found as solutions of the wave equation given appropriate boundary conditions. The usual way of naming and ordering these solutions is by looking at the amount antinodes (peaks and troughs) present in a given direction:

$$\Psi_{mn}(x, y) = \sin\left(\frac{m\pi}{L_x}x\right)\sin\left(\frac{n\pi}{L_y}y\right) \quad (2.6)$$

where m and n respectively are the integer amount of antinodes in the x and y direction, and $L_{x,y}$ the length of the membrane in said direction. The natural frequency of these modes can then be found from

$$\Omega_{mn}^2 = \frac{S}{\sigma} (k_m^2 + k_n^2) \quad (2.7)$$

which is the dispersion relation for the waves [13], where S is the surface tension of the membrane, σ is the surface density, and $k_x = m\pi/L_x$ and similar for n and y , is the angular wavenumber of the wave in x and y . Taking the square root of this expression and using $v = \sqrt{S/\sigma}$ for the propagation velocity of waves through the membrane, we find

$$\Omega_{mn} = v\pi \sqrt{\left(\frac{m}{L_x}\right)^2 + \left(\frac{n}{L_y}\right)^2}. \quad (2.8)$$

Thus clearly, material properties enter into the frequency through the v term at the beginning of the equation: the propagation speed of the waves in the medium. The frequency of the modes scales with the square root of the surface tension, and with one over the square root of the membranes density.

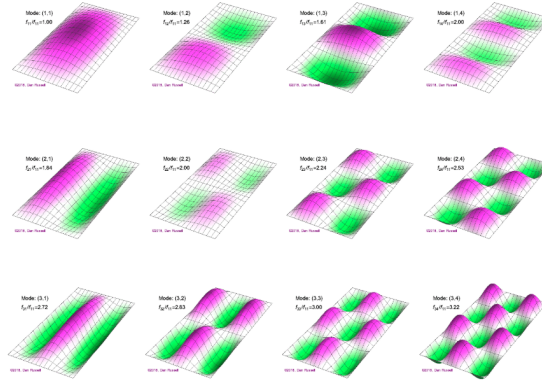


Figure 2.2: Illustration of the first few modes in a rectangular membrane. Courtesy of Dan Russell, [14]

In the following, we will consider only a single mechanical mode, dropping the mode number subscripts m and n , and instead now adopt a subscript m for mechanical, to make absolutely sure to distinguish between mechanical and optical/cavity frequencies.

We can look at the time evolution of the amplitude of this single vibration. Said amplitude ($x(t)$) is described by

$$m_{eff} \frac{d^2x(t)}{dt^2} + m_{eff} \Gamma_m \frac{dx(t)}{dt} + m_{eff} \Omega_m^2 x(t) = F_{ex}(t). \quad (2.9)$$

Here m_{eff} is the effective mass of the vibrating system, equal to the systems full mass if we choose the vibrational amplitude to be the displacement of the systems center of mass; Γ_m is the loss rate of energy from the mechanical mode, referred to as the mechanical damping rate; Ω_m is the frequency of the vibrational mode; and F_{ex} is the sum of all external forces acting upon the oscillator.

The energy loss captured in Γ_m can take many shapes. Most important for our discussion are clamping losses, in which waves within the oscillator are lost into the supports of the oscillator; and viscous damping through interaction with surrounding gas particles. From these earlier quantities, we can introduce another useful quantity: the mechanical quality factor, Q_m .

$$Q_m = \frac{\Omega_m}{\Gamma_m}, \quad (2.10)$$

Being a fraction of the mode frequency and the mode damping, it provides a measure for how quickly the mode loses energy, compared to the energy stored in the mode, or, given the definition used here, more aptly: the fraction of energy lost per cycle (Γ_m), compared to the time it takes for one cycle (Ω_m). Then the quality factor is a quantity describing how many cycles (vibrations) it takes for a system mode to lose all of the energy stored within, and conversely, also for how long it takes for energy to enter the system.

Clearly then, the quality factor is an important measure for our goals: it indicates how well our mechanical system is, inherently, isolated from its environment.

Another important quantity is of course the energy contained in the mechanical system, given by

$$U(x) = \frac{1}{2} m_{eff} \Omega_m^2 \langle x^2(t) \rangle, \quad (2.11)$$

evidently proportional to the square of the displacement. Conversely, the energy in the system is also given by the quantum Hamiltonian, accounting for the energy of each vibrational quantum (usually referred to as a phonon[†]) in the system, given by

$$\hat{H} = \hbar \Omega \hat{n}_m + 1/2 \hbar \Omega_m. \quad (2.12)$$

The quantum mechanical ground state referred to in the introduction corresponds to a phonon occupation (\hat{n}) of 0.

As noted before, energy can and will enter the system from the environment. This must be taken into account when one wants to perform experiments using the ground state. The time it takes for one quantum of energy to enter into the vibrational mode is characterized by what is called the thermal decoherence rate:

$$\hat{n}_{th} \Gamma_m \approx \frac{k_B T_{bath}}{\hbar \Omega_m} \quad (2.13)$$

the rate (Γ_m) at which phonons from a thermal bath (\hat{n}_{th}) leak into the system.

Having established the optical and mechanical system, we will now further discuss their coupling.

[†]Comparable to the photon being a single quantum of electromagnetic radiation

2.1.3 Optomechanical Coupling Between a Cavity and a Membrane

As said multiple times before, the coupling between the optical and mechanical systems is enacted through radiation pressure in the system. We again refer the reader to previous works for mathematical derivation, here sufficing with summarizing the important results.

Specifically for membrane in the middle systems such as discussed in this thesis, the coupling is enacted through a cavity frequency shift due to the dispersive nature of the dielectric membrane. As the position of the membrane changes with respect to the nodes of the standing wave within the cavity, this means that vibrations of the membrane, and the resultant displacement of the membrane relative to the standing wave pattern, lead to a shift in cavity frequency, which can be detected, and which show up as peaks at the vibration frequency in the Fourier transform of the transmitted signal.

An important quantity to take note of is just how much the cavity frequency changes per unit displacement of the membrane,

$$G = -\frac{\partial\omega_{cav}}{\partial x}. \quad (2.14)$$

Multiplying this factor by the zero point motion (indeterminateness of the membranes position in its ground state) x_{ZPF} , we also get the single photon coupling rate, g_0 , providing a figure for how strongly a single photon couples to the mechanical system.

From this, it follows that, at different membrane positions relative to our standing wave pattern, the cavity frequency response will depend upon the displacement differently. Notably, we can position our membrane at either a node or antinode of the cavity field, yielding, respectively, a x proportionality, and a x^2 proportionality. This latter proportionality in turn allows for so called Quantum Non-Demolition (QND) readout of the membranes energy/phonon occupation number (equations 2.8 and 2.9) [10]

Other interesting results include a static shift to the membranes vibrational frequency,

$$\delta\Omega_m = 8\Delta \left(\frac{g_0}{\kappa}\right)^2 \frac{\bar{n}_{cav}^{max}}{[1 + (2\Delta/\kappa)^2]^2} \quad (2.15)$$

This shift results from the introduction of an extra factor to the spring constant due to the radiative pressure of the light.

More generally, one could look at the dynamical effects, of which the previous expression is a limiting case,

$$\delta\Omega_m(\omega) = g^2 \frac{\Omega_m}{\omega} \left[\frac{\Delta + \omega}{(\Delta + \omega)^2 + \kappa^2/4} + \frac{\Delta - \omega}{(\Delta - \omega)^2 + \kappa^2/4} \right] \quad (2.16)$$

and the optomechanical damping,

$$\Gamma_{opt}(\omega) = g^2 \frac{\Omega_m}{\omega} \left[\frac{\kappa}{(\Delta + \omega)^2 + \kappa^2/4} + \frac{\kappa}{(\Delta - \omega)^2 + \kappa^2/4} \right], \quad (2.17)$$

the result of which is optical cooling and heating[‡] of the system. Physically, this can be understood through the coupling between phonons and photons. As a red-detuned photon (lower frequency, lower energy) couples to a phonon, that is thus of higher energy, energy can be transferred more readily from the phonon to the photon than vice versa, leading to a loss of energy in the phonon, and effectively cooling the system. Conversely, for a blue-detuned photon (higher frequency, higher energy), energy is transferred, on average, from the photon to the phonon, up-scattering the phonon and heating the system. The process is shown diagrammatically in figure 2.3.

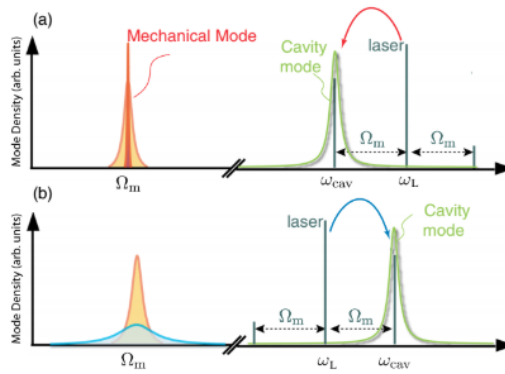


Figure 2.3: Scattering picture of optomechanical cooling and heating, showing the laser line relative to the cavity mode and the resulting up and down-scattered lines at Ω_m relative to it. To the left is the effect on the mechanical mode.

This finishes our discussion of the optomechanics, though many effects still remain. Since they are not of direct interest to this thesis however, the interested reader is referred to textbooks and reviews on optomechanics instead.

2.2 Additional Mechanics of Interest to Membrane Optomechanics

Whilst the most important parts pertaining to the eventual experimental end goal has already been discussed in the previous section, namely the effect of material properties on the membrane frequency (eq. 2.7) thermal decoherence rate (eq. 2.13) and the optomechanical coupling equations (eqs. 2.16, 2.17), some final notes must be made on thermal effects.

2.2.1 Thermal Expansion

Chief amongst these is the principle of thermal expansion of materials. A very straightforward concept, it is simply explained by understanding that temperature is a measure for the vibration of the atoms and molecules constituting a

[‡]Also referred to as driving or amplification.

material. As temperature changes, so does this vibrational amplitude[§]. This in turn means that, as temperature increases, in general, the separation between these constituent parts of the material also will increase[¶], and as such, the material as a whole expands.

2.2.2 Absorption

In this final true section of the chapter, we will go over the concept of absorption, as this is the pathway through which most of the non-optomechanic heating will occur in our system.

The concept of absorption will not be alien to anyone: light traveling through a medium will be attenuated by said medium. Of course the amount of attenuation will be material depended, as light traveling through a clear window will be far less attenuated than, say, light traveling through a glass of milk^{||}.

The principle is clear: absorption is the degree to which a material medium takes energy away from the electromagnetic waves that make up light. The main driver for this loss of energy is found in the interaction between the electric part of the wave, and electrons within the medium.

Absorption of a medium is often quantified through adopting an imaginary part into the materials refractive index. Where the refractive index provides a measure for the propagation speed of light through a medium, and enters as such into the wave equations, a complex component comes into these equations as an exponential decay term. For example, for an electrical plane wave propagating along z with a vacuum wavelength of λ , where we adopt a complex refractive index as $n = n_r + in_i$, we find

$$E(z, t) = \text{Re} \left[E_0 e^{i\left(\frac{2\pi n}{\lambda} z - \omega t\right)} \right] = e^{-\frac{2\pi n_i}{\lambda} z} \text{Re} \left[E_0 e^{i\left(\frac{2\pi n_r}{\lambda} z - \omega t\right)} \right] \quad (2.18)$$

where we recognize an exponential decay of the amplitude in the first term of the final equality. Evidently, this complex term corresponds to the decrease of energy (or amplitude) in the wave as it transverses the medium, which is exactly what we stated the absorption is.

Conclusion of Theory

In this chapter we introduced and explained the concepts of optical cavities and vibrational modes within membranes. We went over their coupling through the radiation pressure and the resulting optical spring effects, and more general mechanical frequency shift and the induced optomechanical damping and driving. We finished the chapter by briefly discussing the concepts of thermal expansion and absorption. In the next chapter we will discuss how these

[§]Or, actually, the other way around, as stated before: temperature can be defined as a measure of exactly this vibrational energy. They are, bar some extra factors, identical by definition.

[¶]Do note that this does only hold in general: in some materials, over some temperature ranges, the converse is true. An example would be water, which is at its densest at roughly 4°C, hence leading to the sinking of the Titanic: frozen ice is less dense than water under normal circumstances, it expands rather than contracts going from 4°C to 0°C. These are, however, definitely the exception, rather than the rule.

^{||}Of course, in both cases, scattering of the light also plays a role and might very well be the predominant driver for loss of light traveling through the milk.

concepts were implemented into the current set-up, how they were used or considered in the design of the new set-up, and how we will attempt to use these concepts to both determine the absorption of the membranes used in our experiments, and to explore possible thermal gradients within our membrane.

CHAPTER 3

Methods

Having discussed the theory underlying this thesis, we will now go over the implementation of those lessons in the experimental set-up in use by the Bouwmeester group in Leiden. We will then introduce the new set-up as first tested in this thesis. After introducing both set-ups, we will go over how to use the former set-up to determine the membrane absorbance and thermal gradient. In principle, the same scheme can be used for the new set-up, provided the new set-up is expanded in a similar fashion to the current set-up.

3.1 The Current Set-Up

As explained in the first section of the previous chapter, an important part of the optomechanical set-up is formed by the optical cavity.

3.1.1 Optical Cavity

In the current set up, the cavity is formed between two commercial Bragg mirrors, in which alternating, quarter wavelength thick, layers of specific optical index are used, matched in such a way that reflections at the consecutive interfaces interfere constructively, providing a transmission of roughly 10 ppm* at the operating wavelength of 1064 nm. Specifically, the system uses curved

*The cavity finesse was measured at around 60×10^3 though, which would indicate that the actual mirror performance lies closer to 50ppm, from

$$\mathcal{F} = \frac{2\pi}{-\ln(R_1 R_2)}, \quad (3.1)$$

indicating a significant amount of absorption somewhere along within the system.

mirrors with a radius of curvature such that the system is nearly[†] confocal when placed at the ends of the cavity, at $R_{1,2} = 5$ cm, and $L = 98$ mm, for the radius of curvature and the mirror separation respectively. This leads to near diffraction limited focusing of the beam at the cavity midpoint, at which the membrane will be inserted. The importance of this for our system specifically will be touched upon in the next subsection, *The Membrane*.

The mirrors are separated by means of a hollow Invar cylinder. the choice for Invar is made since it has a low thermal expansion coefficient, meaning the separation remains stable as the temperature of the cavity is changed. This is of course important for eventual cooling of the system inside a dilution refrigerator, but also simply for room temperature experiments, as it will keep the system robust against temperature drift of the surroundings.

3.1.2 Kinematic Plate and Membrane Holder

The current system also contains a kinematic plate, which allows for tip/tilt positioning of the membrane mount which is attached to it. This is done using a set of three electromotors. This allows for alignment of the membrane perpendicular to the light inside the cavity at focus.

On this kinematic plate, we have mounted the membrane holder, which incorporates a piezo stack to allow the translation of the membrane along z , which, as discussed in the theory, allows us the position the membrane relative to the standing wave pattern of the light within the cavity.

The membrane holder also features an old STM tip (needle) that is bent towards the center of the membrane position, brought to be roughly a hundred micron above the membrane at the end of the tip. Applying an electric potential to this needle polarizes the charges within the membrane (attracting opposite charges and repelling equal charges), which, due to the inverse square scaling of the Coulomb Force law[‡] leads to a net attractive force exerted onto the membrane, as the attracted charges are minutely closer, and thus experience more force. Quickly modulating the applied potential at specific frequencies thus allows us to drive the membrane at those frequencies.

The chip on which the membrane is made is attached to the holder through very soft clamping, using a set of flat copper springs. This soft clamping leads to a decrease in mechanical damping Γ_m through elastic waves, as touched upon in section 2.1.2.

The entire cavity is placed within a vacuum chamber, with light entering through

[†]The choice for a *nearly* confocal system is made due to cavity stability criteria: a confocal system is on the cusp of being unstable, which is to say that if the cavity length of mirror curvature is off by a little bit in the wrong direction, the beam diameter will continuously grow within the cavity, leading to a loss of optical power and information since the beam will be clipped off and lost at the edges of the mirror aperture. The stability criterion can be found as

$$0 \leq \left(1 - \frac{L}{R_1}\right) \left(1 - \frac{L}{R_2}\right) \leq 1,$$

where L is the cavity length, given by the mirror separation, and $R_{1,2}$ is the radius of curvature of the first and second mirror, respectively.

[‡] $F_{Coulomb} \propto \frac{q_1q_2}{r^2}$, sign follows from the sign of the charges, with equal charges repelling, and opposite charges attracting

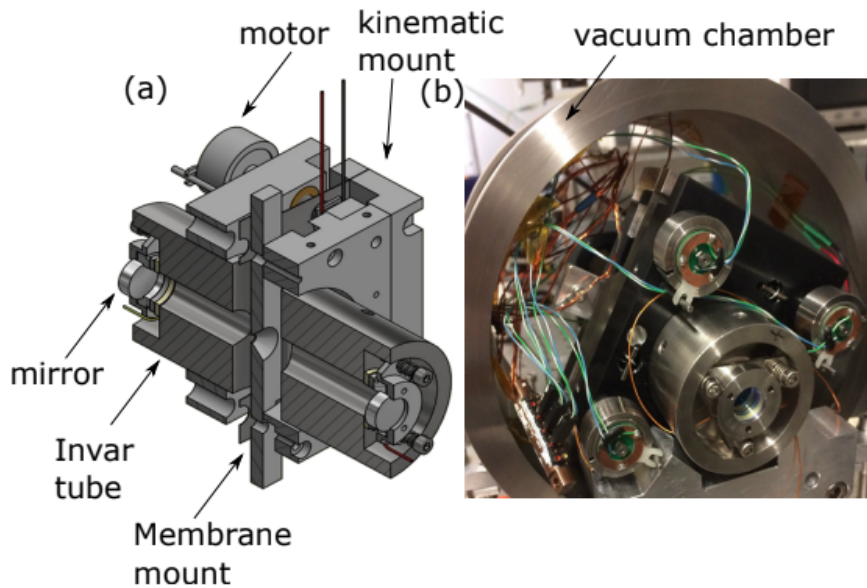


Figure 3.1: AutoCad drawing (a) and image (b) of the current set up, as in use by the group and as used in this thesis. Courtesy of S. Sonar and H. van der Meer

anti-reflection (AR) coated windows. This is done to reduce another major contributor to Γ_m , viscous drag of the air on the membrane. The system is pumped down through use of a prepump and a turbo pump, after which, at a pressure of roughly $1e-6$ mbar, an ion pump is switched on, taking over from the turbopump/prepump combination, which is then decoupled, so as to remove the vibrations caused by the pumps..

3.1.3 The Membrane

The membranes currently in use by the group were fabricated at the University of California, Santa Barbara, by F. Luna. They employ a phononic lattice, which can be seen in image 3.2, which results in a phononic bandgap. That is to say: the structure of the membrane material inhibits phonons at certain wavelengths as they travel through the membrane, effectively not allowing certain wavelength vibrations within the membrane.

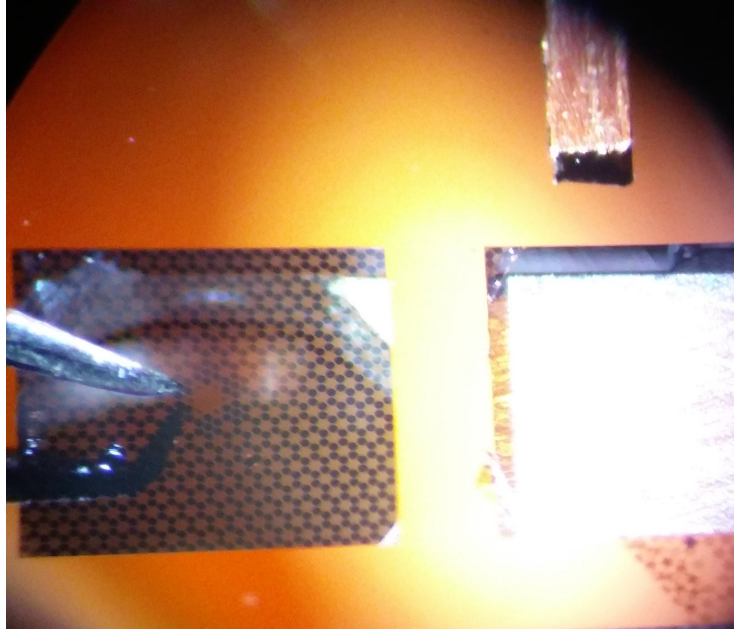


Figure 3.2: Photo of a membrane through an optical microscope. The phononic lattice can be seen on the membrane on the left. The end of one of the copper springs can be seen in the top right. The needle used to excite the membrane can be seen near the center of the membrane, where the defect can also be seen. The needle can be seen brought near the defect, though not completely over it, as this is where the cavity mode should pass through. The orange colour of the background (the Si chip on which the membranes are fabricated, four at a time) is due to reflection of light coming off of the (orange) gloves worn when taking the picture

In the center of the membrane, a defect was created in this structure. In this defect, vibrational modes at frequencies corresponding to those wavelengths are allowed and not inhibited. Effectively, this provides a layer of isolation between those modes and the environment, both trapping the energy of those modes in the center, and keeping external vibrations that could possibly decohere them, out. In theory and practise, this greatly enhances the mechanical Q factor (eq. 2.10) of these so called defect modes through a reduced damping. This lattice is also in part why it is so important for the cavity mode to be focused tightly within the center of the the cavity, as this ensures that the full laser passes through the defect, reducing scattering of light off of the phononic lattice, and going through the most displaced areas of the membrane under vibration, enhancing our sensitivity to the modes of the defect area. This sensitivity is also why the needle is brought as close as possible to the defect area: the Coulomb force falls off rapidly with separation, so for efficient driving of defect modes, the needle must be as close as possible to the defect. The fundamental mode frequency of these membranes lies around 80kHz, with higher frequencies following from eq. 2.8[§]. As noted before, we also have

[§]Equally, since we already know the fundamental mode frequency, we can use

$$\Omega_{m,n} = \Omega_{1,1} \sqrt{\frac{m^2 + n^2}{2}} \quad (3.2)$$

vibrational modes confined to the defect area however, and we can thus distinguish between full membrane modes and defect modes. For defect modes, given the higher Q factor, we find several far more narrow peaks (with peak width at FWHM being equal to the damping rate, similar to the loss rate κ being equal to the optical cavity linewidth) within the range of the bandgap, roughly between 1.1 MHz and 1.3 MHz. The quality factor of these modes lies around 20 mln at the top end, with the quality factor of the 33 full membrane mode at around 900×10^3

3.1.4 The Laser Lab

Having discussed both the resonators (optical cavity and the membrane) of the optomechanical set-up, we still need to discuss the light actually sent into the system.

The system comprises of two lasers, one low powered probe laser used to track the cavities resonance and lock to said resonance and to probe the membrane, and another more powerful drive laser locked to the tracking laser and used to drive the system.

As the cavity modes drift over time due to drifts in temperature and other such influences, the incident light must be locked to the mode we wish to use. This is done using the Pound-Drever-Hall (PDH) technique on the tracking laser, in which one uses the derivative of the reflection signal (which is at a minimum on cavity resonance, as the cavity will transmit on resonance) as feedback to lock the laser to the cavity resonance. As this requires the reflected signal, we use an optical circulator in the path of the optical fiber. The PDH scheme also requires the use of a modulated laser signal, with resultant sidebands. This is achieved through modulation in an Electro-Optic Modulator (EOM) before the probe laser is sent into the system.

Another important part in the optical set up is the Acousto-Optic Modulator (AOM) which, through the use of a crystal and vibrational waves applied to said crystal[¶], deflects the laser beam at increasing angles relative to the incoming light. These sound waves in the crystal can be tuned through an applied voltage to the AOM unit, allowing one to very rapidly tune the amount of light diffracted into a specific mode.

In the set up, this AOM is thus used as a quick switch for the light in optical ring down experiments (which can be used to measure finesse through the cavities decay rate, eq. 2.3), and to create light pulses of specific shapes for more advanced experiments.

The driving laser is locked to the probe laser through an optical phase locked loop (OPLL), in which the beat frequency between the two lasers is kept constant, at a two FSR plus drive detuning separation.

For the details of locking the set-up to the cavity resonance and the PDH

[¶]The waves, and the resulting density fluctuation in the crystal cause a pattern of changing optical index, that is periodic in space. The light is then diffracted of this pattern and comes out constructively interfering with other parts of the light front at increasing angles, into so called modes.

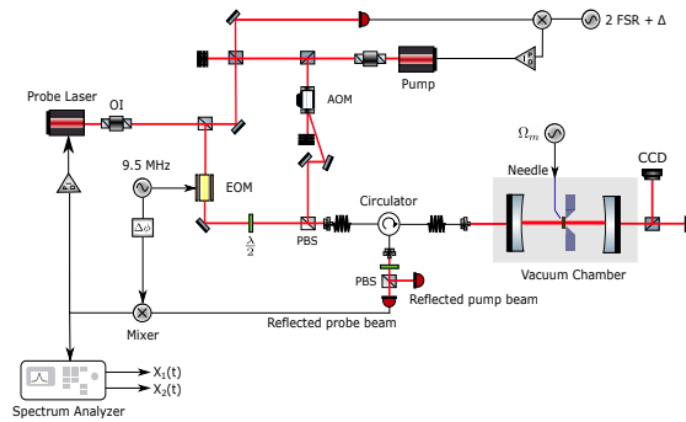


Figure 3.3: Diagram of the optical set-up used for the current set-up. Explanation of the constituent parts given in the main body of text, subsections 3.1.3 (needle) and 3.1.4 (rest). Courtesy of S. Sonar.

scheme as implemented for the set-up, we refer the reader to the thesis of S. Sonar.

The light is taken from the laser lab to the set-up through an optical fiber. The laser is then coupled out of the optical fiber and collimated in the set-up lab, after which it is coupled into the cavity through a coupling lens and a set of mirrors forming a periscope for the alignment of the laser into the cavity.

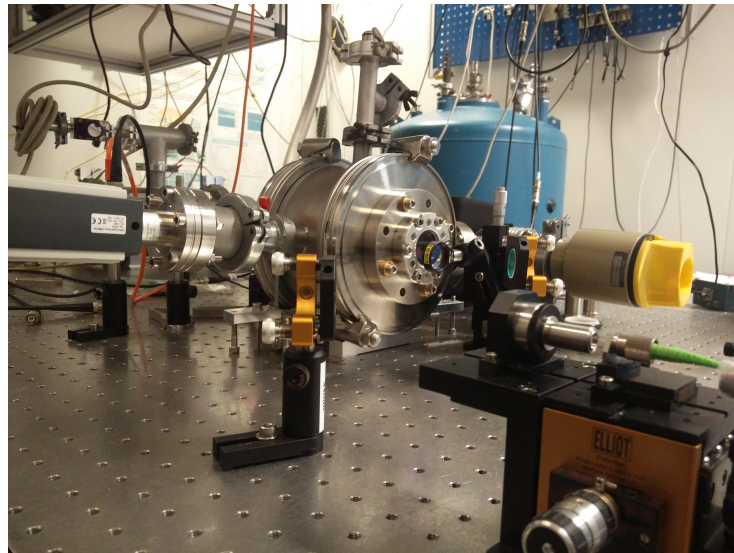


Figure 3.4: Photo of the old set up with the vacuum chamber closed. The fiber launcher and periscope mirrors are visible in the foreground, as is the incoupling lens, positioned just in front of the vacuum chamber window.

Readout of the reflection signal is done by using a photodiode behind a Polarizing Beam Splitter (PBS) connected to a Zurich Instruments Lock-In Amplifier. The PBS ensures that we only measure the signal coming from the probe laser, as the lasers are polarized orthogonally with respect to each other. The vibrational modes of the membrane then show up as peaks in the Fourier transform of the transmission, with the peak area corresponding to the vibrational energy contained within the modes.

3.2 The New Set-Up

The new set-up is very similar to the current set-up. The main difference is the removal of the kinematic plate, as the motors were suspected of inducing drift in the membrane position, and the locking scheme. Since the main laser set-up is in use for the current set-up, we instead used the DL Pro, Tunable Single Diode Laser (Toptica Photonics), without a dedicated driving laser. Rather than using PDH locking at this time, we locked to the side of the transmission peak using the DigiLock software from Toptica Photonics and a DigiLock 110 box (Toptica Photonics). Scanning of the cavity was done through the DigiLock software as well, and the SC 110, Scan Control (Toptica Photonics) unit. In the future, PDH locking will most likely be used.

The mirrors used in the system were rated at 250 ppm transmission at 1064 nm. This results in a lower theoretical finesse of the system ($\mathcal{F} \approx 12500$), and a broader transmission signal. Given that we lock to the side of the transmission peak, the broadening of the transmission peak actually helps us with our locking.

The end mirrors are also fixed onto the set-up somewhat differently in the new set-up. Where the mirrors were clamped in the old set up using screws and springs similarly to how they are clamped in the new set-up, some major changes were made as well. The Invar housings of the mirrors are clamped onto a smooth Invar surface in the new set-up, see figure 3.5, and a set of four screws, two for each of x and y, on each side allow for very gentle displacement of the mirrors through sliding of the housing across this surface.

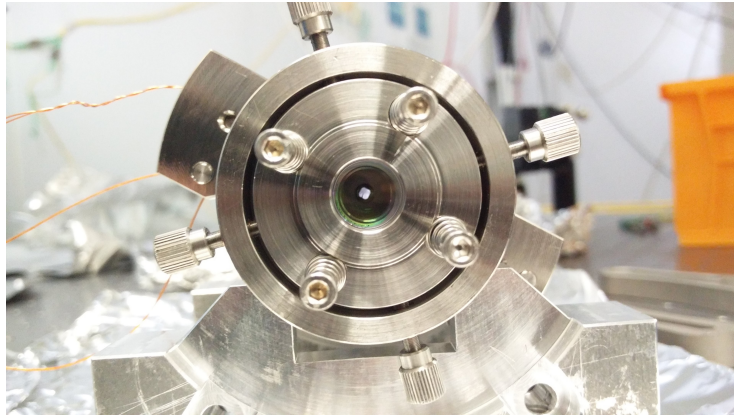


Figure 3.5: The Invar housing of the front mirror, as described in the text. The screws to displace it can be seen on the photograph as well. The angle is slightly of horizontal, this will be discussed in the next chapter, Results. The copper wires that can be seen coming out of the cavity are the twisted pair of ground and needle for the electric excitation of the membrane and the wires connected to the piezo stack of the membrane holder.

The set-up uses a vacuum system similar to the current set-up, with a drum chamber with AR coated windows at both ends, pumped down using a pre-pump and a turbopump, and held at vacuum using an ionpump (Agilent).

The membrane chip is fixed to an Invar holder, as seen in figure 3.6. The piezo stack is placed between two plates, with the Si chip clamped to the top plate using the soft, flat, copper springs.

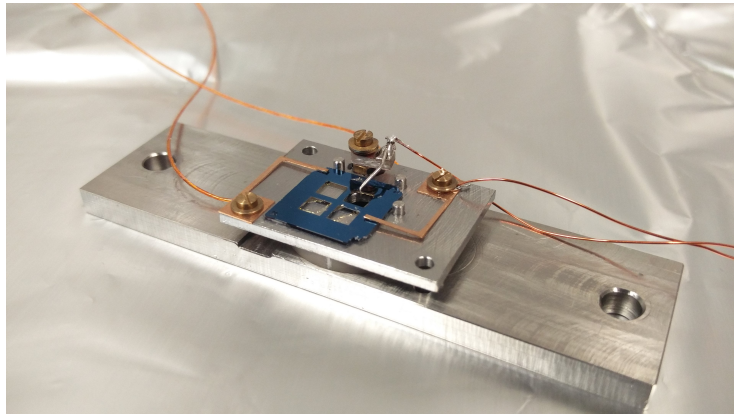


Figure 3.6: Membrane holder as described in the text.

The needle we attached above the membrane can also be seen, though more clearly in figure 3.7. A small piece of PCB functions as the base of the old STM needle, from which it is gently bent using tweezers to be just above the membrane. The PCB can then be turned through the screw, which screws into a nut that was affixed to the holder with Stycast. This rotates the needle to

be above the chip, and near the defect mode of the membrane under test. To ensure this movement is steady, a set of bent washers are used as springs.

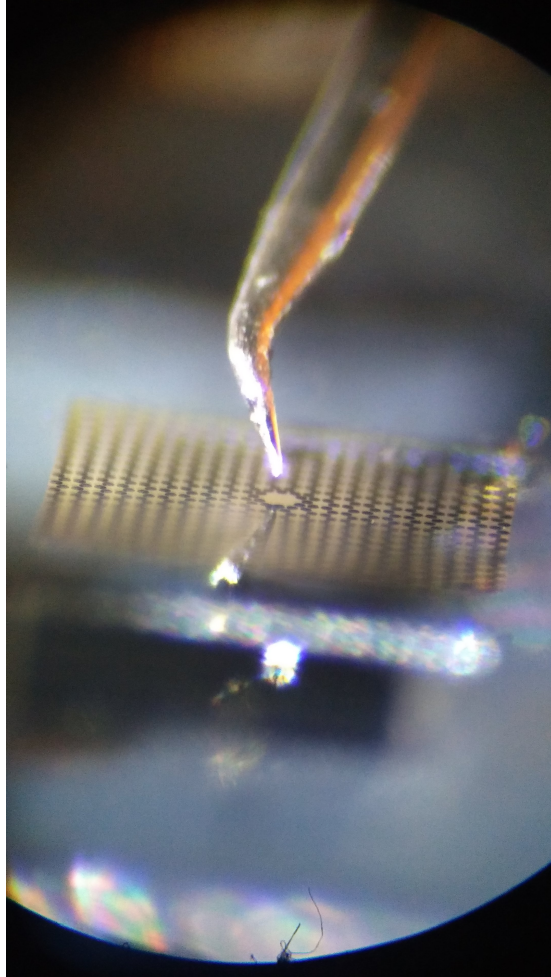


Figure 3.7: The needle placed near the defect mode, as seen through an optical microscope.

3.3 Absorbance Measurement

As was noted in the theory, subsection 2.2.2, the main pathway through which energy from light is absorbed within media, is through interaction between the material and the electric part of the electromagnetic wave. Since our membranes are very thin, at 25 nm for the latest generation, the electric field amplitude within the membrane can vary greatly between different membrane positions, since the field has a wavelength of 1064 nm, which means there is 266 nm between a peak in the field strength, and a node, a good ten times the thickness of our membrane.

We can use this property of our system, as this allows us to, effectively, regu-

late the amount of energy absorbed by the membrane. At the antinodes of our standing wave pattern, the absorption will be maximal, whereas, at the nodes, it will be minimal^{||}. As this absorption will enter into κ as an extra loss factor, it will enter into the cavity finesse as well, through eq. 2.3.

Consequently, one can, provided known cavity parameters, fit the theoretical finesse vs membrane z to actual finesse vs z data acquired from the working system including the membrane. This could yield the imaginary part of the membrane refractive index, when used as the fitting parameter, and so obtain the membranes absorption. This scheme was shown by A.M Jayich et al [15].

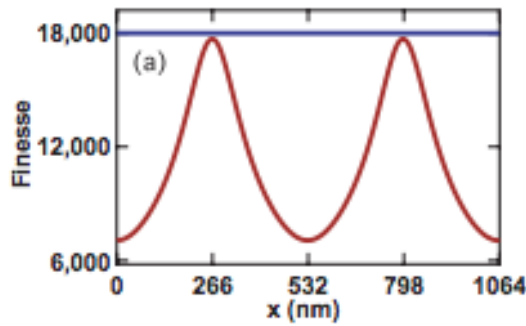


Figure 3.8: Figure taken from [15], depicting a finesse vs. membrane position curve for a membrane without absorption (blue line, $n = 2.2$) and a membrane with $n = 2.2 + 1.5 \times 10^{-4}i$.

To obtain the cavity finesse, one could either record the transmission peak line width, which is proportional to κ , and thus to the finesse, or one could do optical ring down measurements, in which optical power in the cavity is allowed to build up, to then quickly switch off the incident power (in our scheme, using the AOM) and record how long it takes for the power in the cavity to fall off and from this time constant, τ , calculate the finesse, using $\mathcal{F} = \Delta\omega_{FSR}\tau$. For high finesse cavities, optical ring down measurements are preferable [16]

3.4 Thermal Gradient Measurement

Whilst our membrane's thermal conductance at room temperature will most likely be sufficient to rapidly carry away any thermal load from our membrane, with only minor heating, it is unsure, and in fact unlikely, that this will be the case at cryogenic temperatures, where the main pathways of heat transport are "frozen out". In fact, it can be seen that thermal conductivity of SiN membranes tends to zero as temperatures drop below 10 K [17].

This means that we must take measures to ensure sufficient heat conductivity as the temperature is lowered. One possible measure to take would be the deposition of a thin metallic film onto the membranes. Metals are in general very

^{||}Do note that, obviously, the material property *Absorbance* will not be changed with the membrane positioning. It is this property that is captured within the imaginary part of the refractive index used in eq. 2.18.

good heat conductors, so a thin film could ensure adequate heat conductivity to counteract heating from absorption.

Depositing such a metallic film would however spoil the membrane properties. Therefore, we would like to keep any such film as minimal as possible. This means that we must be able to measure the effectiveness of such a film, that is, how effectively the membrane is thermalizing.

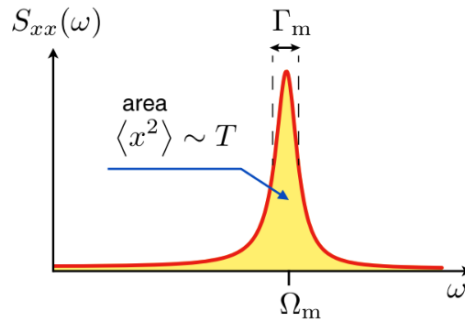


Figure 3.9: The Fourier Transform of the signal coming back from the cavity provides us with the noise spectrum of the membrane. The area of the peaks in this spectrum are proportional to the temperature experienced by that vibrational mode. Figure courtesy of [8]

As can be seen in figure 3.9, the area of the spikes of the mechanical modes in the Fourier transform of the optical signal is proportional to the temperature of the mode. Using this, one could probe the temperature of the membrane: if one makes sure not to cool or drive the membrane optomechanically, this temperature of the mode is the average temperature of the membrane. One could then take a measurement at room temperature and very low laser power (to ensure there is truly no heating from the incident laser) to determine the factor of proportionality.

This by itself tells us whether the membrane is heating up, but not per se whether this is due to bad heat conductivity. For this we must leverage the specifics of our membranes.

Since our membranes have both full membrane modes, and defect modes, we could, in principle, use these to determine a temperature gradient. If a temperature gradient is present in the membrane, and this is caused by heating at the laser focus in the center of the membrane, the defect modes will experience a higher effective temperature compared to the full membrane modes, as they are confined to the center of the membrane. This could be determined from determining the area of the modes in the noise spectrum.

In principle, one need not even determine the factor of proportionality, as a scaling difference for increasing applied heat would already indicate the presence of a temperature gradient. Taking a room temperature measurement is however hardly time consuming.

Results and Discussion

In this section we will go over the results of this thesis. We will follow the order as given in *Methods*. The results will be discussed here as well.

4.1 The New Set-Up

The new set-up was first characterized without a vacuum chamber.

4.1.1 First Alignment

The alignment of the system proved relatively straight forward, starting off by using a visible red laser source* and pin holes to overlap back reflections coming from the flat face of the front mirror and the both curved mirror surfaces. The alignment of the flat face was done by adjusting the periscope, after which the alignment of the curved surfaces was done by moving the end mirrors. Moving the end mirrors through the use of the screws proved to be mostly stable at this stage of the alignment.

Having aligned the visible reflections, the next step was to use a higher wavelength source. Using the tunable wavelength source, we start off far detuned ($\lambda \approx 950nm$), where a set of points show up on the camera on the transmission side. When scanning the laser slowly, these spots reveal interference fringes. By moving the front and back mirrors in x and y , these spots can be made to overlap, with each spots movement roughly corresponding to movement of one of the two mirrors. As the spots are made to overlap more closely, the movement of their interference fringes with equal laser scanning increases.

4.1.2 Final Alignment

Increasing the wavelength from 950 nm to roughly 1000 nm, we start seeing Hermite Gaussian modes appearing. Scanning the laser slowly, we find the fundamental TM00 mode visually, and optimize the signal of this mode by

*The mirrors, being fabricated for 1064, are not very reflective at this wavelength, giving very low cavity finesse and allowing us to clearly see the reflections from the front and back mirror separately, as spots of increasing size.

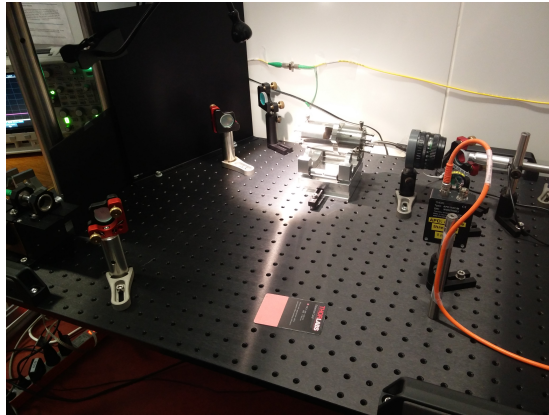


Figure 4.1: Set-up without the vacuum chamber. Periscope and fiber collimation seen to the left, white light for imaging the membrane seen towards the top. A lens is used to refocus the light transmitted through the cavity, after which it is sent through a beam splitter to be imaged with a camera in one arm, and sent to a high speed detector in the other arm.

looking at the brightness on camera, and it's peak on the oscilloscope. We do this several times, slowly increasing our wavelength up till 1064. It is somewhere at this point that small issues start arising with the new method for aligning the end mirrors. Since the plate holding the mirrors is circular, a displacement over one axis can also lead to a displacement over the other axis. After all, as the circle is moved from the center, the screws on the other axis stay at a separation given by the diameter of the cylinder, but cylinder will be less thick in the line of the screws at its new position. This leads to much frustration and instability of the alignments whilst aligning. When the desired position is achieved, the screws on the other axis can and must be re-tightened, but this is also not without risk, as this can shift the mirrors again. We would recommend flattening of the actuation points of the screws, giving a flat work surface over some ± 2 mm.

At this point, we again find the TM₀₀ mode at 1064 nm, and now maximize it's signal by tweaking the periscope and the beam collimation (the z knob of the xyz stage from which the fiber is launched). Doing this, we could regularly achieve a maximum transmission signal without in coupling lens of about 300 mV, which corresponds to a transmission of about 2% with the laser going out of the laser lab at roughly $100\mu W$ [†]. The actual transmission of the cavity will most likely be better, since it is likely more power was lost between the laser lab and coupling into the cavity.

The most important loss in this case, however, is most likely the lack of a mode matching lens and the resultant coupling of the Gaussian wave front into the cavity modes, with the laser beam diameter being very small going into the cavity.

[†]APD110C/M detector (Thorlabs), which has a responsivity at 1064 of roughly 7A/W, and, when terminated at 50Ω resistance, a 50kV/A transimpedance gain. A peak height of 300 mV corresponds to a current of $6 \times 10^{-6}A$, which corresponds to a transmission signal of $0.86\mu W$. Since this is the transmission measured in only one arm of a 50/50 beam splitter, we can double this, to roughly 2% of the incoming light.

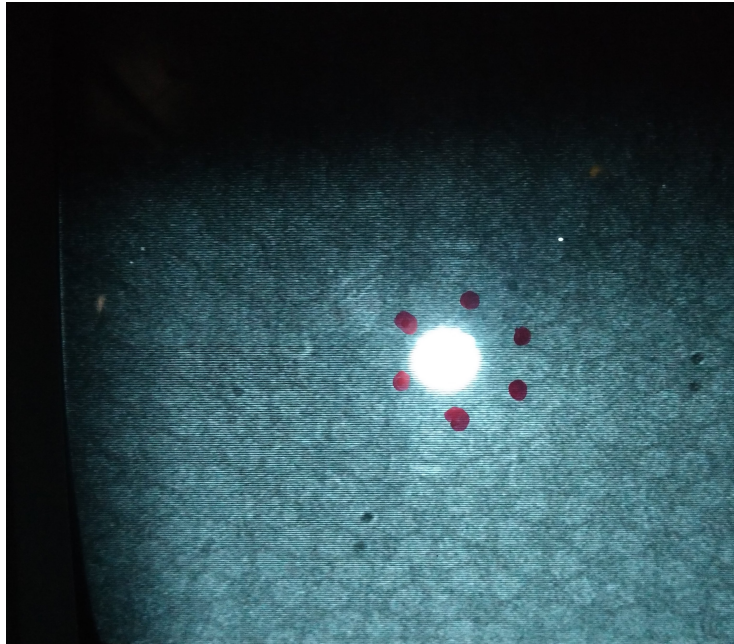


Figure 4.2: Camera image of the TM00, fundamental Gaussian cavity mode, imaged together with the membrane on a small camera behind the cavity. The red dots are placed at the edges of the defect. The refresh rate of the monitor and the moiré patterns made taking clear images difficult.

4.1.3 Empty Cavity Finesse

At this point, we measured the finesse of the cavity using optical ring down measurements on the TM00 mode. Fits to the time constant of this ring down put the cavity finesse at roughly 20 000, which is considerably better than what the mirrors were rated for, putting the mirror transmission closer to 160 ppm.

4.1.4 MiM

We then inserted the membrane, making sure the TM00 mode went through (as best as we could) the center of the membrane defect.

To check this, we used white light going through a pinhole and a (set of) lens(es) to image the membrane on the camera placed behind the cavity. This proved to be quite a pain at times, mostly due to the light source being suboptimal, and the path into the system not being clear (sending it either through the back of one of the mirrors of the periscope, or reflecting it off the mirrors mount). This could be improved by adding a flip mirror to send the white light into the optical path, though this would mean we can no longer image both the membrane and the optical modes simultaneously.

Alignment of the membrane with the modes could be achieved by subtly shifting the membrane holder within its clamps on the cavity.

At some times, this was however not possible, notably so when the cavity

modes were slightly below the center of the structure: whereas moving the holder up and to the right was possible, pin made to rest the holder on made it impossible to do the same down and to the left.

In practise, this meant that one should set the optical modes somewhat off towards the right-top for fine tuning later on, and pre-image the membrane on the camera and record where the defect would end up. In doing this, the cavity mirrors hardly changed the path of the white light used to image the membrane anyway, so there was no big issue when the cavity mirrors were subsequently shifted to align the cavity.

An adaption that should be considered for this and current versions is to place these pins somewhat further back. The pins are useful for resting the holder on whilst working on the system and should not be removed, but they are not necessary to keep the holder in place. This is taken care of by the screws clamping the holder to the cavity.

Ideally, one would of course make sure that the defect is truly in the center of the cavity, given asymmetrical thermal expansion when the system is cooled down. For more on these considerations, we refer the reader to the thesis of M. Fissicaro.

4.1.5 MiM Finesse

Having so aligned the membrane, we took cavity ring down measurements again. Having repeated this entire process over multiple full realignments, it became clear that the correct alignment of the system was very important. In some measurements, we found the maximum MiM finesse (having scanned the z displacement of the membrane using the piezos) to be almost identical to the empty cavity finesse, at $19\,600 \pm 200$ and $20\,000 \pm 100$ respectively. In other measurements, however, we found similar empty cavity finesse ($18\,000 \pm 200$), but with the MiM finesse being much further removed ($14\,000 \pm 400$). The spread on those measurements was also considerably higher. A possible explanation for this would be that the membranes tip/tilt was off, causing an increase of losses in the TM₀₀ mode, and possibly even the mixing in of higher order, lower finesse Hermite Gaussian modes.

4.1.6 Tip/Tilt Alignment

Aligned to the best of our abilities, we found a misalignment of the membrane reflection of about 2 mm on a pinhole at a separation of about 400 mm for the visible red laser. Using Snell's law and a ray trace diagram including only the first cavity mirror as a plano-concave lens, this works out to a membrane misalignment of roughly 700 arcs, where we assumed that the incoming ray was perfectly along the optical axis of the mirror. This agrees with alignment bounds given by other groups, at ± 825 arcs being allowable [10]. Other papers talk of far more stringent requirements though, at ± 5 arcs [15]. Given that we achieved near similar finesse empty and MiM, it would seem that the less stringent requirements are sufficient for at least our cavity with the current mirrors. If higher reflectivity mirrors are used, however, and the finesse resultingly increases, this might no longer be the case.

Since the kinematic plate was removed from the system, there is no way to change the tip tilt of the membrane. Rather, the system has to be aligned to the cavities tip tilt. The issue with this, however, is that this means that the front mirror of the cavity does double duty: it is used both to align the cavity properly to the incoming beam, and it changes the angle of the cavity modes relative to the membrane.

It seems that this is in fact a workable situation to at least the current finesse, but some form of tip tilt system for the membrane might be required to truly leverage a higher finesse system.

The finesse vs displacement characteristics of these membranes in this cavity will be discussed in a later section, 4.2.

4.1.7 Vacuum

Having tuned the cavity, we placed it within the vacuum chamber. Having displaced it somewhat relative to the periscope in doing so, we retuned the periscope, usually getting similar transmission signal after doing so, indicating that the loss from the AR coated cavity mirrors is indeed minimal.

The system was then pumped down to roughly $1\text{E-}6$ mbar. At first, we did not yet have an ion pump, so some first measurements of cavity locking and the membranes noise spectrum were done whilst attached to the prepump/turbopump set-up, which revealed that the system was relatively stable, being able to lock and find mechanical modes even with the vibrations from the pump, on a table top set-up without the usual optical table. Eventually an ion pump was used and the turbopump was decoupled, however, as described in the *Methods* chapter.

4.1.8 Membrane Modes PSG5_1_1,3 and PSG5_2_1

We locked the laser to the TM00 mode as described in the methods, though with the laser detuned to 990 nm, as the transmission peak was too narrow to successfully lock to at higher wavelength (due to the resultingly higher finesse of the cavity at those wavelengths) and then recorded the transmission signal[‡]. As described before, the vibrational modes of the membrane show up in the Fourier transform of this transmission signal as peaks at the vibrational frequencies. Without exciting the system, we could clearly see the fundamental mode of the membrane at around 77 kHz, as a broad thermal peak. We also saw some other modes, and some unwanted peaks. One of these peaks, at 82.5 kHz, corresponds to the lighting in the lab and disappears as this is turned off. Two other peaks seem to be artifacts from the lock-in amplifier, at 57.57 kHz and 91 kHz.

If we apply a modulated voltage to the needle, we see that the peaks corresponding to mechanical modes grow considerably, confirming that the needle works.

At one point we used the piezo in the mount to excite the membranes. Given

[‡]The width of the transmission peak was roughly 10 mV of the laser scan, of which 6.3 V corresponds to a single FSR. From this, we find a cavity finesse of roughly $\mathcal{F} \approx 600$ with the detuned laser

the inefficiency of this procedure, this required considerable modulation. Worse, given our soft clamping of the membrane chip, the chip shifted, and our optical mode no longer went through the defect.

Using the needle to drive the membrane however, we used the ZI-sweep function to find other modes. Here the ZI Lock-In amplifier applies a voltage to the needle, modulated at a ramping frequency, and records the response of the membrane at that frequency, effectively giving us the peaks of the modes as they are resonantly driven.

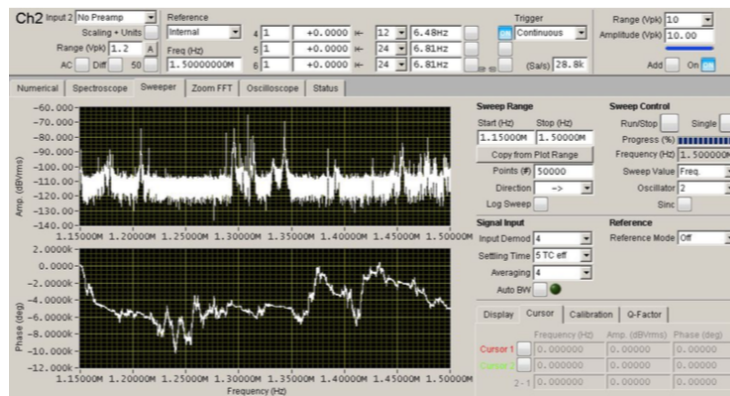


Figure 4.3: ZI-sweep of the bandgap area. It is clear that there are quite a few peaks in here, many of which of low quality factors.

Using this we found the membranes 33 mode ($\Omega_{3,3}$) at around 237kHz, which roughly corresponds to 3 times the fundamnetal frequency, which is what we would expect from eq. 3.2. This 33 mode is of importance to the work currently done in the group, as it is used in STIRAP experiments for state control and transfer in eventual quantum superposition experiments in which different membrane modes are to be brought into a super position.

4.1.9 Bandgap

Exploring membrane PSG5.1.1, we found that the membrane's phononic lattice seemed to be under performing. The same seemed the case for PSG5.2.1. Membrane 5.1.3 was damaged before we could test it further. Compared to previous membranes (PSG4.1.1), there seem to be far more peaks in the frequency range of the bandgap, which seems to lie around 1.15MHz to 1.45MHz for the devices in question.

Some relatively narrow peaks were found in the bandgap nonetheless.

4.1.10 Quality Factor

The quality factor of these peaks and of some peaks outside the bandgap were determined through mechanical ring down. Using the needle to drive the modes and then turning off the needle potential, we recorded the decay time of the modes on the oscilloscope. The time τ it took for the amplitude to half

was used to calculate the Q factor,

$$Q = 4.5\Omega_m\tau \quad (4.1)$$

which gives us, for PSG5.2.1

Ω_m	τ	Q
79.54 kHz	780 ms	270 k
237 kHz	2.7 s	2.88 mln
1.415 MHz	810 ms	5.14 mln

In which the 33 mode looks promising, surpassing the Q-factor of the membrane currently in use by the current set-up, but the Q-factor of the best defect mode, at 4.7 mln, is much lower than the Q-factors of comparable modes in the current set-up, at around 14 mln.

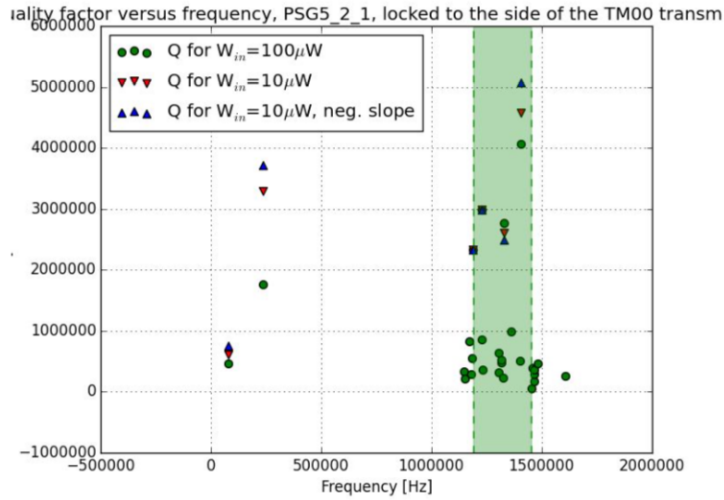


Figure 4.4: Plot of the Q factor for various modes in the PSG5.2.1 membrane.

This, combined with the presence of junk peaks (low, broad peaks) in the bandgap, would indicate that the phononic lattice of the membranes was damaged. Indeed, for PSG5.1.1, this was visually confirmed, with a small section of the bandgap, away from the defect, displaying a small tear.

4.1.11 Frequency Dragging and Optical Driving

Whilst sweeping the peaks, we saw frequency dragging of the modes, following from eq. 2.18.

We also found that locking on the blue side of the transmission peak proved far harder, though not impossible. If monitored on the oscilloscope, the motion of the membrane modes could be seen to increase when locked to the blue side.

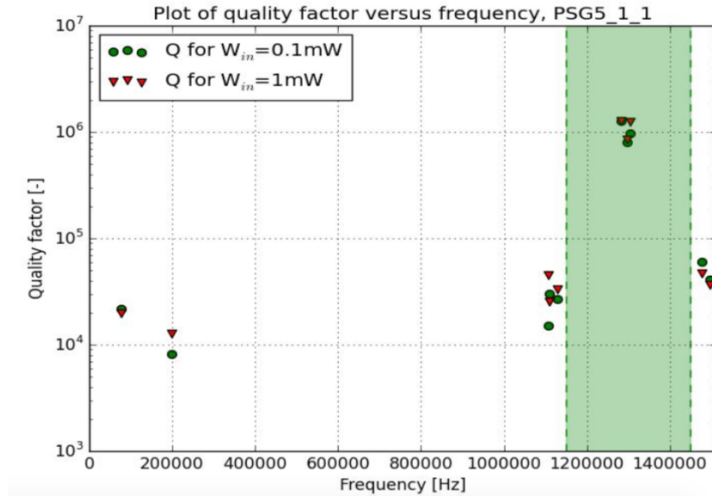


Figure 4.5: Plot of the Q factor for various modes in the PSG5.2.1 membrane.

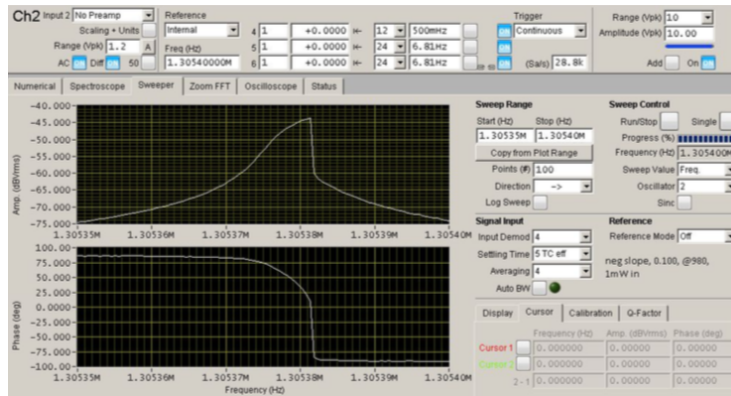


Figure 4.6: Sweep of a peak showing clear frequency dragging, with the mode frequency being "dragged" in the direction of the sweep.

We attribute this to the optical driving of the mode, following from eq. 2.17. It is clear that, even detuned to far lower finesse than possible, optomechanical effects were already quite strong. A final note to be made was an observed downward drift of all the membranes frequencies over time. In this thesis we have not studied this, though we expect that this is the result of the considerable strain present in the membranes from fabrication slowly releasing.

4.2 Membrane Absorbance Measurements

Measurements of the finesse versus membrane position for PSG5.1.1 showed finesse falling only by about 10%, from 20 000 to 18 000 roughly, which seems to indicate that this membrane does in fact have relatively low absorption (with

literature reporting typical values of such SiN membranes in the range of 10^{-4} on the high end, to 10^{-6} on the low end). Comparing these characteristics, this would presumably place the membrane towards the low end. This was for the new set-up with the PSG5 membranes however, where we did not accurately record the the finesse vs z curve.

We did try to record it for the current set-up, where we sought to determine it from the width of the transmission peak. The response of the transmission signal to membrane position was so strong however, that the lock was lost multiple times whilst attempting to take the measurements. We attempted, in the end, to only record the peak width at the high transmission points, which would coincide with the high transmission points, as was also done in previous papers.

After acquiring the data and putting it together, however, it became clear that something had gone wrong. As can be seen in figure 4.7

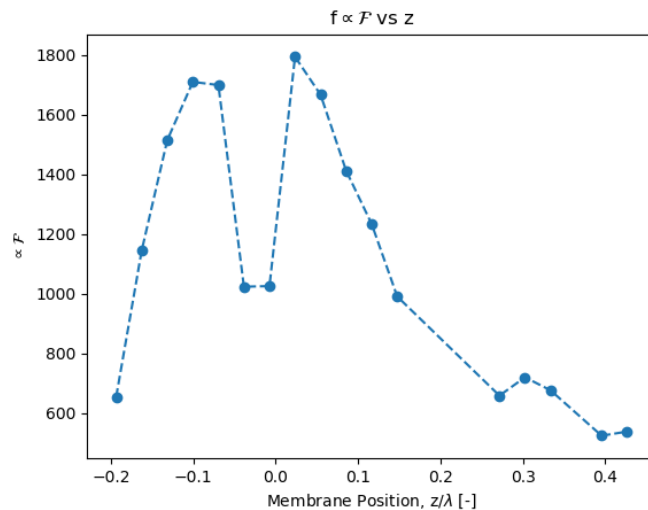


Figure 4.7: Plot of $1/\text{FWHM}$ as acquired from the oscilloscope transmission peak versus the membrane position in fractions of the wavelength. Peaks would be expected with a separation of $1/2$, coinciding with the nodes of the standing wave and minimal absorption. The FWHM seen here, as taken from the oscilloscope was not converted to be equal to κ . In principle this could be done easily through taking a cavity ring down measure of the finesse, but at that point, one has to wonder why you would not just use ring down to acquire all the data.

Part of the explanation for this would be locking to the wrong mode after losing the lock. We did not look at the beam profiler after locking. It is therefore possible that we locked to a higher order, lower finesse mode of the cavity. We also observed some drift of the membrane position in the cavity over time as well, through a changed laser detuning and a change in our transmission signal whilst we did not vary the membrane position ourselves. This was also seen before, which is in part why the new set-up was developed.

All in all, the data acquired was not sufficient to determine the absorption of the membrane, though it is most likely towards the higher end of the scale, since the system responds strongly to a change in membrane position. The system also displayed considerable amounts of drift, which made the linewidth method for determining the finesse somewhat unfeasible.

4.3 Thermal Gradient Measurements

Measurement of the thermal gradient was attempted as well, but ran into similar issues, where the drift of the cavity mode relative to the laser lead to vastly different amounts of laser detuning between even consecutive measurements. The resultant difference in optomechanical damping lead to vastly different values for measurements that were supposed to be at the same temperature. When plotted and averaged over several measurements (16 measurements per run, 10 runs per data point), the error bars proved to be decent.

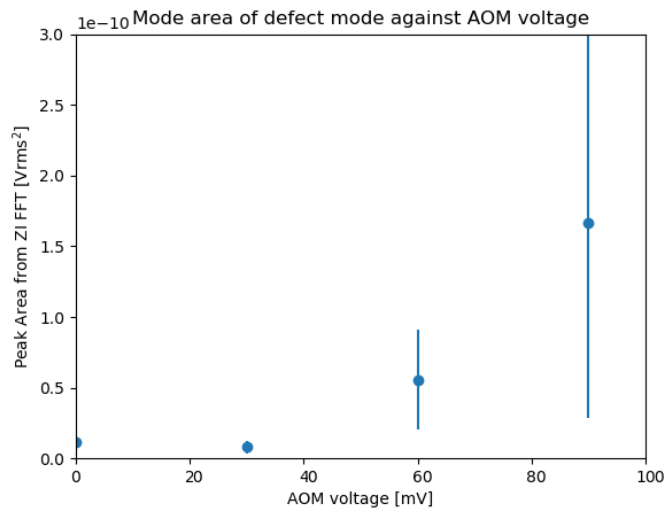


Figure 4.8: Mode area of the defect versus Voltage applied to the AOM. The incoming power is a function of the AOM voltage.

For the defect mode, we see nonlinear scaling. This could be correct, however, since the AOM only scales linearly at higher applied voltages. The decrease in mode area from no power to 30mVDC is also as expected, since we performed our measurements slightly red detuned, so as to properly lock to the cavity. Ideally we would lock at zero detuning, but due to drift, this was unfeasible, so cooling the mode was the lesser of two evils for this measurement.

The increase in mode area is as one would expect if heating is taking place in the membrane due to the incident power of the laser. If we are to calculate a proportionality constant between temperature and mode area, taking the 0 power mode at 300 K, we find unphysical results: the high power temperature would come out to above 4000 K, which would be well above the melting point

of Silicon Nitride. Most likely, this is due to a change in optical damping between the measurements having a very strong effect on the mode area. As noted before however, an absolute temperature correspondence is not strictly needed though, as we more so care about a difference in scaling between the different modes.

Looking at the full membrane 33 mode, we find that something seems to have gone horribly wrong when measuring the 30mVDC value. Presumably, the membrane was driven at some point of that measurement, probably due to the aforementioned drifts.

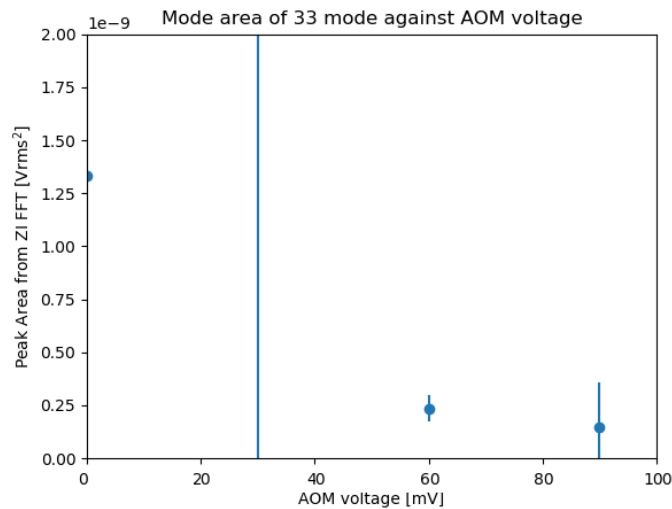


Figure 4.9: Mode area of the 33 mode versus Voltage applied to the AOM. The 30mVDC value clearly deviates and should be discarded.

Removing said point, we are left with a downward trend on the membrane, rather than an upward one. This curve looks clearly different from the curve we found for the defect mode. However, given the instability of the detuning, and the clearly enormous effect of said detuning, we must be very careful drawing any conclusions from this, all the more so since the data points for the 33 mode and the defect mode were acquired consecutively, and not simultaneously.

Whilst a clear scaling difference can be seen, it is, given the lack of system stability, not feasible to say we have actually shown a temperature gradient at this time.

4.4 Mode Frequency Drift

As noted before, downward drifts in frequency were observed in the membrane over time. We will not discuss this (slow) drift here. Rather, we will discuss a far quicker observed drift in the membranes frequency.

The drift in frequency seemed to coincide with incident laser power being switched on, reaching a steady state after some time. Through use of some

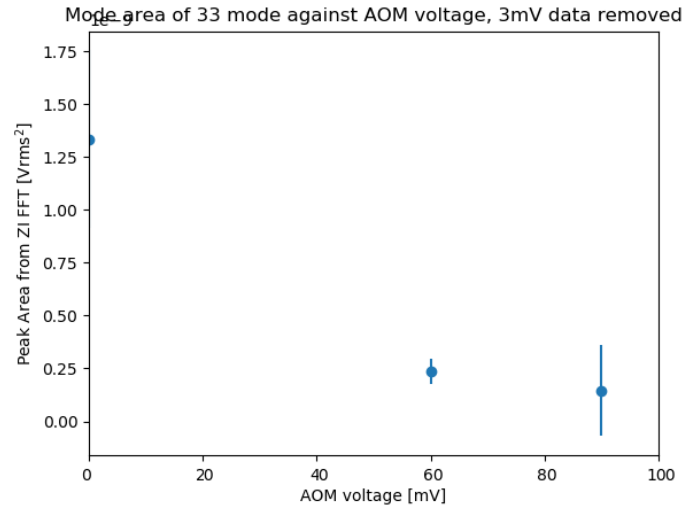


Figure 4.10: With the 30mV point removed, the points seem to show a downward trend.

matlab code, we tracked the mode frequency of the defect mode and the 33 mode of the membrane, as can be seen in figure 4.11.

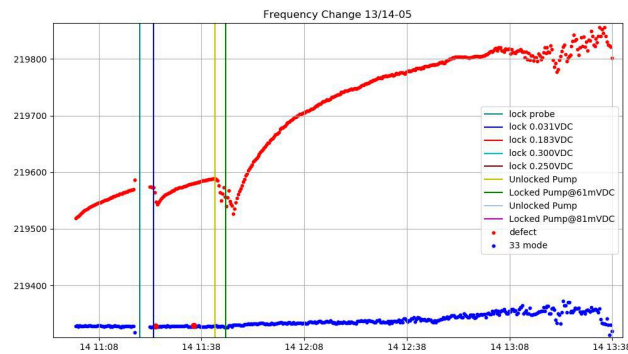


Figure 4.11: The mode frequency of the defect mode as plotted here was shifted down by 1040000 Hz for ease of plotting. The actual mode frequency lies around 1.26MHz.

The drift after switching on the pump laser at 61mV to the AOM tends toward a steady state. Equilibrium is reached after the frequency went up by some 300 Hz. Given a nominal mode frequency of 1259500 before the drift, this amounts to a change of roughly 24 ppm. When looking at the 33 mode data, there seems to be no drift whatsoever. Zooming in seems to reveal a very small drift however,

The cloud at the end of the measurement does not coincide with the shape of the drift on the defect mode, and does not seem sensical. This cloud is probably from faulty acquiring, or drift on the lock and can be disregarded.

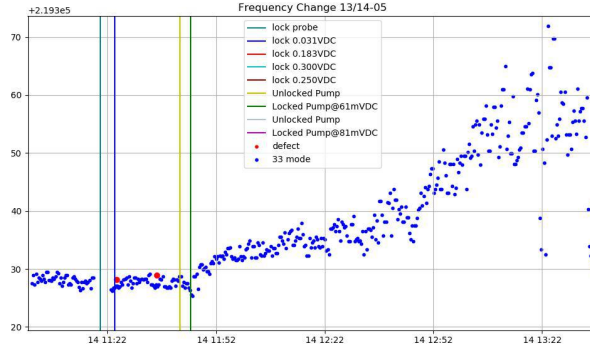


Figure 4.12: A zoom in on the frequency track for the 33 mode. Whilst nothing seems to happen after the laser is switched on at 31mVDC to the AOM, something seems to happen when this is increased to 61mVDC.

There is, however, a small increase just after switching on the laser where the shape does coincide with the shape displayed by the defect mode frequency change. In this bit, the frequency climbs by some 10 Hz, or about 4 ppm.

Since the response of the defect mode also seemed to be related to the power of the incoming beam, a possible suspect would be thermal effects. For the defect mode, the total response time seems to be around 1 hour, whereas it was much lower for the possible shift in the 33 mode, at 10 minutes.

To determine if it could be a thermal effect we will do some back of the envelope calculations, to establish a decent estimate. We will assume that the absorption of the membrane is in line with similar membranes used by other groups, which gives us a range of

$$n_i \in [10^{-6}; 10^{-4}]. \quad (4.2)$$

This would mean that our membrane absorbs [150 ppb; 15 ppm] of all light incident on it. Then, assuming that an AOM voltage of 61mV coincides to roughly $10\mu W$, and an intra cavity power amplified by the finesse, $\mathcal{F} = 60000$, this gives a thermal load on the membrane as

$$Q \in [0.09\mu W; 9\mu W]. \quad (4.3)$$

Using thermal properties for SiN membranes found in [17], we find that the dissipation for the full membrane lies at around $1\mu W/K$. For the defect mode, due to the heat having to traverse half of the membrane to get to the Si chip heat bath, this number lies around roughly $0.2\mu W/K$.

That is to say, for low membrane absorption or low laser power, the full membrane would be expected to not heat up much at all, as the dissipation seems the keep up with the heating (in the above worst case, we would get about a 10 K raise in temperature). For the central region of the membrane however, we would expect a raise in temperature for all but the absolute best case. This best case is extremely unlikely, as explained in section 4.2.

Having established then that it is likely for the temperature to rise in the membrane as the pump laser is turned on, and more likely so for the defect mode still, we must establish what effect this could have on the membrane frequency. The first suspect would be thermal expansion. In the case of Silicon Nitride at room temperature, the coefficient is firmly positive, which would mean that any heating would release strain from the membrane (SiN membranes are highly stressed from their fabrication). Following eq. 27, such a strain release would rather *reduce* the frequency of the mode.

From literature, it also seems the the thermal expansion of the Si wafer should be lower than that of the membranes [18], so expansion of the wafer relative to the membranes as a cause seems unlikely.

A final explanation could be thermal expansion of the chip holder plate, which could, through the clamping, exert a force resulting in an increase in tension in the membranes. Heating of the holder plate would, assuming it is made of Invar, take roughly 3.4 J/K, assuming the insulation around the piezo provides thermal insulation from the rest of the cavity. Given the above proposed thermal load, heating with a magnitude of 1 to tens of Kelvin could be possible.

If the plate is actually made of Invar, however, the thermal expansion of the plate would again be in line with the Si chip, and this would fail to explain the drift.

CHAPTER 5

Conclusions

5.1 The New Set-Up

For the new set-up, it can be concluded that it is stable and mostly well alignable. The only issues with alignment are the lack of tip/tilt correction of the membrane, which will become a larger problem with higher cavity finesse, and the small instability during alignment due to the screws actuating on a curved surface.

The membranes tested in the new set-up showed issues due to damages, precluding real work on the defect modes and drastically reducing the Q-factor of said modes, whereas the full membrane modes were hardly affected.

We also observed optomechanical driving and cooling and demonstrated optomechanical frequency drag, even when detuned from the high finesse region. The measured PSG5 membranes had damages, which probably lead to the failing of the bandgap. They did, however, display superior quality of the 33 mode, when compared to the membrane currently in use by the group. It would therefore make sense to finish the new set-up (that is to say, add the PDH scheme to it, and add in the higher quality mirrors) and move to new membranes with that set-up.

5.2 Membrane Absorption

Cavity ring down seems to be better suited for measuring the finesse, and should in future be used if one is to determine the membrane absorption.

The drift in the system and the loss of locking in the current set-up made acquiring the finesse through FWHM measurements unfeasible.

From measurements on the PSG5 membranes, it seems that these membranes have lower absorption when compared to the membrane currently in use in the current set-up. Perhaps this is due to the "salt" that was still on the PSG4 membranes when they arrived in Leiden. This salt was later cleaned off, but it is possible that this either left residue, or in some other way negatively affected the absorption of the membrane.

5.3 Thermal Gradients

Whilst a clear scaling difference can be seen between the two modes, it is, given the lack of system stability, not feasible to say we have actually shown a temperature gradient at this time.

To be able to conclude this, either the detuning stability should be improved, or at the very least, mode area measurements should be further automatized and taken, preferably simultaneously, or at the very least, in an interleaved fashion. That is not to say that the method has proven unfeasible, however. Rather, the optomechanical effects should be minimized. Perhaps one could even use a high powered laser at a wavelength that is not resonant with the cavity to provide the heating, if disentangling the optomechanical from the thermal effects proves too hard.

5.4 Mode Frequency Drift

Whilst we proposed some solutions and attempted to find a clear suspect through some estimations, the real answer eludes us. The effect does seem to be thermal, given the relatively slow response time (since if it was some sort of optical spring effect, the response would be near instantaneous).

Some weird interplay with the phononic lattice seems unlikely, since the full membrane mode also seems to display the drift, albeit to a smaller degree, and only at higher incident power.

In principle, the frequency drift can be handled by continuous tracking, or, since it approaches a steady state provided constant power, wait time. If one is to use pulses to establish state transfer and entanglement however, as is the goal, this becomes more problematic. Ideally, then, one would isolate the source of the drift, and possibly eliminate it through either better thermalisation, or some other measure.

Acknowledgements

I would like to thank many people for the many things they did for me and with me during my master thesis.

First and foremost, I would like to thank Dirk, not only for giving me the opportunity to do this research, but also for the nice conversations I've had with him, both during and before this project.

I would also like to thank Wolfgang, both for valuable discussion and help with the idea of my thesis, and for his presence at lunch, where he always brought interesting topics to the table, and a warm smile.

Perhaps most, I would like to thank Vitaliy, who was always available to answer questions, even when he was away on holiday. Whilst I sometimes had trouble gauging how you felt about things, you always seemed kind and you have an infectious smile!

Whilst we did not work together much, I also want to thank Fernando, who fabricated the membranes used in this thesis. I'm sorry I damaged some of them, but I don't think you would ever get mad.

Furthermore, I would like to thank everyone else that was on the 9th floor during my project. Lunch was usually a busy affair, often also due to me perhaps, but it was, without a doubt, good fun. And sometimes even informative.

I would like to thank Gesa, who helped me when my vacuum system seemed to be on the fritz. The same goes for Federica, both for her help (and a lot of acetone and isopropanol, thanks Federica!), and also for nice conversations and the occasional jokes.

I want to thank Norman and Jimi for entertaining me when my cavity did not cooperate.

I am also very happy Matteo joined us, and would like to thank him, both for helping me take my measurements, and for discussing much of the project with.

To all the other people outside of university, Marieke, Sara, Rik, Jessamy and Georgy, my parents and my sister, I would like to thank all of you, for all the little things you did for me, with or without your knowledge.

References

- [1] R. Jozsa and N. Linden, *On the role of entanglement in quantum computational speed-up*, Proceedings of the Royal Society of London. Series A: Mathematical, Physical and Engineering Sciences **459**, 2011 (2003), arXiv: quant-ph/0201143.
- [2] E. Schrödinger and J. D. Trimmer, *THE PRESENT SITUATION IN QUANTUM MECHANICS: A TRANSLATION OF SCHRÖDINGER'S "CAT PARADOX PAPER"*, page 25.
- [3] CDC, *CDC | Facts About Cyanide*, 2019, <https://emergency.cdc.gov/agent/cyanide/basics/facts.asp>, 2019-08-22.
- [4] D. Ellerman, *From Abstract Entities in Mathematics to Superposition States in Quantum Mechanics*, arXiv:1701.07936 [physics, physics:quant-ph] (2017), arXiv: 1701.07936.
- [5] H. Lüth, *Quantum Physics in the Nanoworld: Schrödinger's Cat and the Dwarfs*, Springer Science & Business Media, 2012, Google-Books-ID: Sr-sweYrNVgkC.
- [6] R. P. Crease, *The double-slit experiment*, 2002, <https://physicsworld.com/a/the-double-slit-experiment/>, 2019-08-22.
- [7] G. Gasbarri, M. Toroš, S. Donadi, and A. Bassi, *Gravity induced wave function collapse*, Physical Review D **96**, 104013 (2017), arXiv: 1701.02236.
- [8] M. Aspelmeyer, T. J. Kippenberg, and F. Marquardt, *Review Optomechanics.pdf*, REVIEWS OF MODERN PHYSICS **86**, 1391 (2014).
- [9] W. Marshall, C. Simon, R. Penrose, and D. Bouwmeester, *Towards Quantum Superpositions of a Mirror*, Physical Review Letters **91**, 130401 (2003).
- [10] J. D. Thompson, B. M. Zwickl, A. M. Jayich, F. Marquardt, S. M. Girvin, and J. G. E. Harris, *Strong dispersive coupling of a high-finesse cavity to a micromechanical membrane*, Nature **452**, 72 (2008).
- [11] S. Sonar, *Multimode Optomechanics with a Membrane-in-the-middle System*, PhD thesis, Leiden University, IIT Bombay, 2018.
- [12] E. Vlieg, *A membrane-in-the-middle device for optomechanics*, PhD thesis, Leiden University, 2017.
- [13] D. Morin, *2D waves and other topics*, page 11.
- [14] D. Russell, *Rectangular Membranes*, 2018, <https://www.acs.psu.edu/drussell/Demos/rect-membrane/rect-mem.html>, 2019-08-22.

References

- [15] J. G. E. Jayich and A. M. Harris, *Dispersive optomechanics: a membrane inside a cavity*, *New Journal of Physics* **10**, 28 (2008).
- [16] M. C. Darrow, *Finesse Measurement in Fabry-Perot Interferometers*, (2014).
- [17] H. Ftouni, C. Blanc, D. Tainoff, A. D. Fefferman, M. Defoort, K. J. Lulla, J. Richard, E. Collin, and O. Bourgeois, *The thermal conductivity of silicon nitride membranes is not sensitive to stress*, *Physical Review B* **92**, 125439 (2015), arXiv: 1506.01838.
- [18] C.-L. Tien and T.-W. Lin, *Thermal expansion coefficient and thermomechanical properties of SiN_x thin films prepared by plasma-enhanced chemical vapor deposition*, *Applied Optics* **51**, 7229 (2012).